We are IntechOpen, the world's leading publisher of Open Access books Built by scientists, for scientists

6,900
Open access books available

185,000
International authors and editors

200M
Downloads

154
Countries delivered to

Our authors are among the
TOP 1%
most cited scientists

12.2%
Contributors from top 500 universities

CLARIVATE ANALYTICS
BOOK CITATION INDEX
INDEXED

WEB OF SCIENCE™

Selection of our books indexed in the Book Citation Index
in Web of Science™ Core Collection (BKCI)

Interested in publishing with us?
Contact book.department@intechopen.com

Numbers displayed above are based on latest data collected.
For more information visit www.intechopen.com

Computational Study of A15 Ru-Based Alloys for High-Temperature Structural Applications

Bhila Oliver Mnisi, Evans Moseti Benecha
and Meriam Malebo Tibane

Abstract

The structural, magnetic, electronic and elastic properties of A15 X_3Ru (X = Sc, Ti, V, Cr, Mn, Fe, Co, Ni, Cu and Zn) binary alloys are investigated using first-principles density functional theory (DFT) methods. Ru-based alloys have attracted remarkable research interest due to their unique properties, which make them suitable for high-temperature structural applications. In this chapter, the properties of several A15 Ru-based alloys are investigated in order to select the best suitable alloy/s for aerospace application. Heats of formation are calculated to determine the thermodynamic stability of the materials. Knowledge of the values of elastic constants is essential for understanding the mechanical properties of the materials. From our calculated elastic constants, the bulk modulus, shear modulus, Young's modulus, Poisson's ratio, melting temperature, anisotropic factor and the ratio B/G are determined. The electronic density of states are calculated and discussed. Lastly, the magnetic properties of A15 X_3Ru alloys are studied. Thermodynamically stable Mn_3Ru possesses high-magnetic moment compared to other X_3Ru alloys, these results could pave way to experimental realization (synthesis) of Mn_3Ru material.

Keywords: structural stability, heats of formation, DFT calculations, mechanical properties, 3d transition metal alloys

1. Introduction

High-temperature structural materials have attracted considerable interest in the world of materials research for many years. There is a huge demand for materials that can resist extreme mechanical, thermal and chemical environments. Ni-based super-alloys (NBSA) are currently used for high-temperature application due to their phenomenal properties such as high creep strength, good ductility at elevated and room temperature environments, low density and high melting points. Despite the accomplishment of NBSA, 90% of Ni's melting point have already been exploited [1]. Many metal alloys are currently being studied [2] as potential alternatives to NBSAs.

Currently, ruthenium (Ru) based alloys have been under intense study [3, 4] due to their attractive combination of physical and mechanical properties, including

high melting point and good oxidation and corrosion resistance. Furthermore, Ru has the capability to increase the microstructural stability of other material systems [3]. In particular, Ru (2334 °C) has a superior melting point compared to Ni (1543 °C), making Ru-based alloys suitable for high temperature structural applications. Previously in Ru–Cr phase diagram, many structures such as Cr_3Ru, Cr_2Ru and Cr_4Ru phases were found to exist experimentally in different temperature formations [4–6], while the narrow homogeneity range of 31.5 atm% Ru and 32–36 atm% Ru for A15 Cr_3Ru and Cr_2Ru (σ phase) have been identified by Venkatraman and Neumann [7] respectively. Recent studies in this class of alloys have projected phase stability in a several X-Ru (X = Mo, Ti, V, Hf, Ir, Os, Pt, Ta, Tc, Mn and Zn) binaries at low temperatures [8, 9]. Ruthenium alloys with platinum and palladium make extremely durable electrical contacts and resistors. Ruthenium thin films are used in hard disk drives and plasma display panels [8]. The addition of ruthenium improves the mechanical properties and corrosion resistance of titanium, platinum, palladium, gold, and nickel-based superalloys used in jet engine turbine blades [10]. Also, the addition of ruthenium in modern nickel superalloys inhibits the formation of topographical closed packing (TCP) phases, thereby extending their creep capability to higher temperatures [11–13].

In this chapter, the structural, magnetic, electronic and elastic properties of the A15 Ru-based alloys in the X_3Ru (X = Sc, Ti, V, Cr, Mn, Fe, Co, Ni, Cu and Zn) crystal phase are investigated using first principles density functional theory calculations. All the structures proposed here in A15 phase are new except A15 Cr_3Ru that exist experimentally [7] as stated above. Therefore more experimental research is needed specifically for these novel alloys studied herein. We determine the heats of formation, density and magnetic moments, these properties are very important in aerospace and spintronic applications. Stability study based on heats of formation can be used to identify suitable X_3Ru material for high temperature structural application. The electronic properties such as band structures and density of states are useful to provide valuable information about a material's conducting characteristics at the Fermi energy level. Knowledge of the values of elastic constants (C_{ij}) is crucial in describing the mechanical resistance in a crystal when external stresses are applied. From the C_{ij}'s, we can determine the bulk, shear and Young's modulus that provides information about the strength of the material. To gain deeper understanding of X_3Ru alloys, we compute more properties such as anisotropic factor and Poisson's ratio. The computed properties are compared with the available theoretical and experimental results. The results found herein will pave way to recommend new metals in elevated temperature applications.

2. Theoretical calculations by density functional theory (DFT)

2.1 Crystal structure of transition metal-Ru alloys

Ru-based intermetallic alloys exist in different crystal structure phases such as A15, DOc, DO'_c tP16, $L1_2$, and B2. However, in this chapter we will focus on A15 Ru-based alloys as illustrated in **Figure 1**. The X_3Ru (X = Sc, Ti, V, Cr, Mn, Fe, Co, Ni, Cu and Zn) crystallizes in a cubic A15 type with a space group Pm-3 N (number 223) and a theoretical lattice constant of 4.63 Å [14]. Moreover, this cubic phase possess a prototype of Cr_3Si. The A15 phases are described as a series of intermetallic compounds with a formula A_3B; where A is a transitional metal and B can be any element. In the case of X_3Ru, Ru and X represent the A and B respectively. The proposed study seeks to model the properties of 3d transition metal-Ru
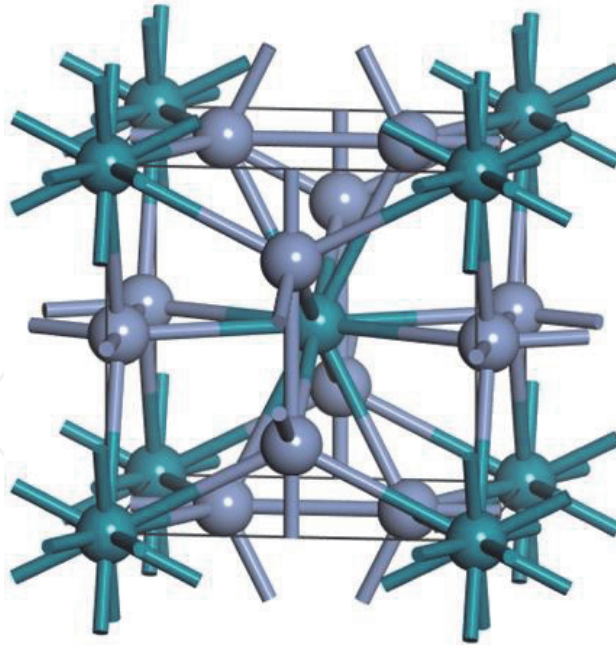
Figure 1.
Ball and stick illustration of A15 crystal structure phase of X₃Ru alloys. Gray balls represent X = Sc, Ti, V, Cr, Mn, Fe, Co, Ni, Cu and Zn- atoms; green balls represent Ru- atoms.

intermetallic systems for A15 phase, using density functional theory techniques. The density functional theory enables determination of many ground state properties of material systems with sufficient accuracy, and is widely used in characterizing the properties of new materials.

2.2 Quantum mechanical techniques

In material science, the energy of a system is needed in order to evaluate the properties of a material. Numerically, this is obtained by solving the Schrödinger wave equation [15].

$$H\psi = E\psi \tag{1}$$

where H is the Hamiltonian operator, E is the energy of the particle and ψ is the wavefunction is the particle's wavefunction. Hamiltonian H in Eq. (1) for a system of many interacting particles (electrons and nucleus) can be expressed as

$$H_{ele-nuc} = T_{ele} + T_{nuc} + V_{ele-nuc} + V_{ele-ele} + V_{nuc-nuc} \tag{2}$$

where T_{ele} and T_{nuc} are the kinetic energy operators of the electrons and nuclei respectively, $V_{nuc-nuc}$, $V_{ele-ele}$ and $V_{ele-nuc}$ are potential energy operators of the ele-nuc, ele-ele and nuc-nuc, respectively, due to Coulomb interactions. Eq. (2) can be solved analytically for few atoms, however, for very large number of atoms ($N \sim 10^{23}$) it is intractable to solve; hence, a number of approximations are needed to find its exact solution. The first approximation in solving the Schrödinger equation for a many-body interacting system is called the Born and Oppenheimer approximation [15]. This approximation decouples the electron motion from that of heavier ions, setting the kinetic energy operator of the nuclei to zero, while the potential energy operator becomes a constant. The Born and Oppenheimer approximation reduces the complexity of Eq. (2) to

$$H_{ele-nuc} = T_{ele} + V_{ele-nuc} + V_{ele-ele} \tag{3}$$

To solve the Eq. (3), the last two terms: $V_{ele-ele}$ and $V_{ele-nuc}$ must be known. Quantum mechanical techniques, such as the density functional theory and the Hatree-Fock approximation aim to obtain accurate ground state energy of a material system comprising of electrons and nucleus. Thereafter, other properties related to the total energy of the system can be easily determined. In order to achieve this aim, the exact forms of the terms on the right hand side (RHS) of Eq. (3) must be known. All the terms are known except the exchange correlation energy of interacting electrons that remains unknown. The density functional theory accounts for the electron exchange correlation (E_{xc}) effect for many interacting particle system. However, the Hatree-Fock has difficulties in predicting the properties of metallic and magnetic systems accurately.

2.3 Density functional theory

The density functional theory minimizes the difficulty in strong electron-nuclei and electron–electron interactions in many body systems (Eq.(2)) by mapping it onto the single particle moving in an effective potential [16]. This effective potential is not explicitly known, but can be approximated to accurately predict the solid-state properties. The basic idea of the DFT is that any property of a system of many interacting particles can be expressed as a functional of the ground state electron density $\rho(r)$.

$$E = E[\rho(r)] \tag{4}$$

DFT is established from the Hohenberg-Kohn theory [16], which expresses a one-to-one correspondence between the electron density $\rho(r)$ of a many electron–electron interacting system and the external potential V_{ext} imposed by the nucleus. Thus, the accurate ground state wave function is obtained from the external potential expression due to a correct ground state electron density. Therefore, the minimum energy can be expressed as:

$$E[\rho(r)] = T_{ele}[\rho(r)] + F_{HK}[\rho(r)] + V_{ext}[\rho(r)] \tag{5}$$

where, $F_{HK}[\rho(r)]$ is the universal functional of the electron density due to kinetic energy $T_{ele}[\rho(r)]$ and potential interactions $V_{ele-ele}$. The universal functional is called the Hohenberg-Kohn density functional and can be expressed in terms of the interaction from the electron-exchange and correlation and Hatree potential V_H due to classical electrostatic interactions [17] as:

$$F_{HK}[\rho(r)] = T_{ele}[\rho(r)] + \int \frac{\rho(r')}{|r - r'|} dr' + V_{xc}[\rho(r)] \tag{6}$$

where, the first term is the kinetic energy of the non-interacting electron system, second term is the Hatree potential V_H and the third term is the exchange-correlation potential due to electron-nuclei interactions.

Now the total energy can be written as:

$$E[\rho(r)] = T_{ele}[\rho(r)] + \int \frac{\rho(r')}{|r - r'|} dr' + V_{xc}[\rho(r)] + V_{ext}[\rho(r)] \tag{7}$$

where, the last two terms are external potentials that are split into two categories namely: classical and non-classical energies due to the nuclei $V_{ext}(r)$ and exchange-correlation effects $V_{xc}(r)$.

Eq. (7) can be written as:

$$H_{KS}\psi_i = \left(-\frac{\hbar^2}{2m_e}\nabla^2 + \int \frac{\rho(r')}{|r-r'|}dr' + V_{ext}(r) + V_{xc}(r) \right)\psi_i(r) = \varepsilon_i\psi_i(r) \qquad (8)$$

Eq. (8) is called the Kohn-Sham energy equation for non-interacting particles. The Kohn-Sham equation substitutes the many body interacting particle into a single independent particle equation as a functional of the ground state charge density, where ψ_i is the single particle Kohn-Sham wave function. The ground state density can be then be described as:

$$\rho(r) = \sum_{i=1}^{N} |\psi_i|^2 \qquad (9)$$

whilst the exchange-correlation potential, V_{xc} (r) is given by the functional derivative of the ground state total energy with respect to the ground state charge density:
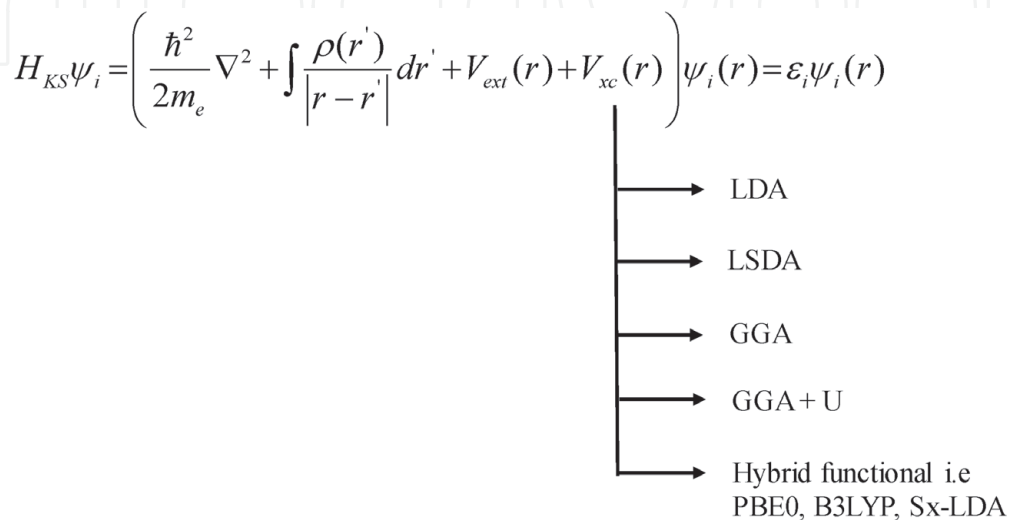
$$V_{xc}(r) = \frac{\delta E_{xc}[\rho(r)]}{\delta\rho(r)} \qquad (10)$$

2.4 Approximations to exchange-correlation functional

While the DFT is in principle an accurate theory describing ground state interactions in a many-particle system, in practice, approximations are needed to describe the electronic exchange correlation term in the Kohn-Sham Eq. (8). Therefore, the application of DFT depends on the accuracy and reliability of the approximations to the exchange correlation potential, V_{xc}. Consequently, a large number of exchange-correlation functionals, including the LDA, GGA, and other hybrid functional have been developed in order to obtain a numerical solution to the Kohn-Sham equations, as illustrated in **Figure 2**.

2.4.1 Local density approximation

The simplest approximation to the exchange-correlation term in the Kohn-Sham equations is the Local Density Approximation (LDA) [15]. LDA assumes the density

$$H_{KS}\psi_i = \left(\frac{\hbar^2}{2m_e}\nabla^2 + \int \frac{\rho(r')}{|r-r'|}dr' + V_{ext}(r) + V_{xc}(r) \right)\psi_i(r) = \varepsilon_i\psi_i(r)$$

LDA

LSDA

GGA

GGA+U

Hybrid functional i.e
PBE0, B3LYP, Sx-LDA

Figure 2.
Kohn-sham-DFT equation and its methods of implementation.

of homogeneous electron gas with a slowly varying electron density gradient, for the exchange correlation functional, expressed as [16].

$$E_{xc}^{LDA}[\rho] = \int \rho(r)\varepsilon_{xc}(\rho(r))dr \tag{11}$$

where ε_{xc} is the exchange-correlation energy per electron in a homogenous electron gas. One of the limitations of the LDA approximation is that it does not account for in homogeneities in electron density resulting in overestimation of bonding energies in both molecular and solid systems. Then Local spin density approximation (LSDA) [15, 17, 18] improves Eq. (11) by including the effect of spin density, where the charge density is the total summation of spin up α and down β densities.

$$E_{XC}^{LSDA}[\rho] = \int \rho(r)\varepsilon_{xc}(\rho_\alpha(r), \rho_\beta(r))dr \tag{12}$$

2.4.2 Generalized gradient approximation

The generalized gradient approximation (GGA) functional is an improvement over the LDA, which takes into account the gradient of the electron density $|\nabla\rho|$ as well as their magnitude at each point r.
Therefore, the total energy can be expressed as a functional of the gradient of the density as

$$E_{XC}^{GGA}[\rho] = \int \rho(r)\varepsilon_{xc}(\rho(r), |\nabla\rho(r)|)dr \tag{13}$$

Inclusion of the information on the electron density spatial variation in GGA results in greater flexibility in describing real materials. However, GGA is inadequate in describing the properties of strongly correlated material systems, such as transition metals and magnetic systems. In order to improve the accuracy of GGA, an additional term called the "Hubbard U parameter" is used to treat the delocalised and localized orbitals with strong on-site coulomb interactions. The Hubbard U parameter is usually obtained semi empirically, but can also be extracted from ab initio calculations, although both methods do not permit transferability of U across compounds. The GGA + U functional will be used in this study owing to its accuracy and relatively minimal computational cost compared to non-local hybrid functionals such as B3LYP, HSE03 and Sx-LDA.

2.5 Numerical solution of Kohn-sham equation

To solve the Kohn-Sham single particle equation, the electron wave function ψ_i for the orbitals must be known. The Kohn-Sham equations are solved iteratively within a self-consistent field, where an initial density $\rho_1(r)$ is "guessed" to obtain the starting wavefunctions. These variables are then used to build Kohn-Sham Hamiltonian of which an improved density $\rho_2(r)$ is obtained. The wavefunctions continues to obtain better approximations to the electron density $\rho_{3\ldots\ldots N}(r)$, until self-consistency is reached, as illustrated in **Figure 3** [19].

2.6 Mechanical properties

Mechanical stability is a measure of material's strength, and is used to characterize the structural stability and deformation of a system under external load [18].
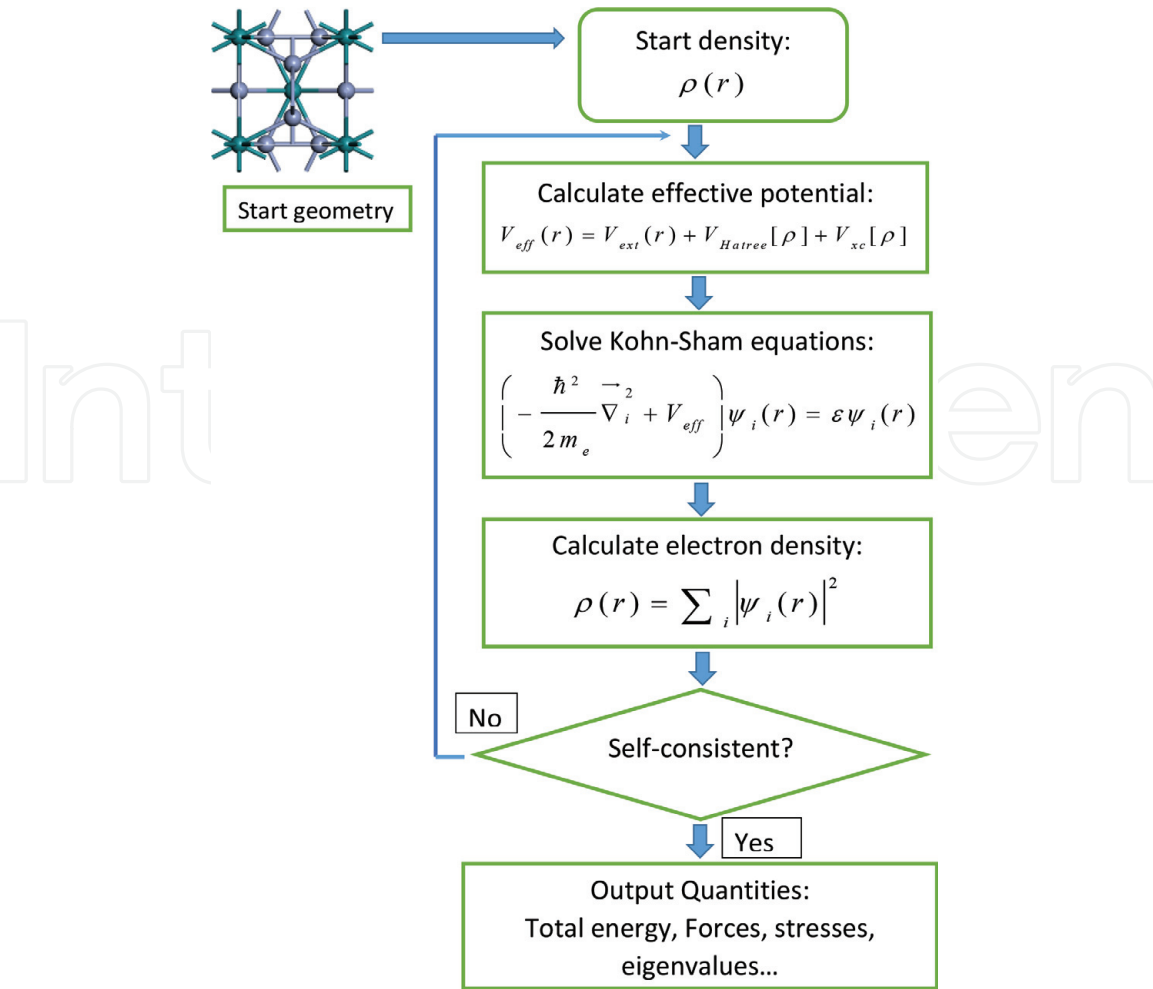
Figure 3.
Schematic representation of the SCF method used in DFT.

Material's mechanical stability is defined in terms of elastic constants C_{ij}, Bulk Modulus (B), Shear Modulus (G), Young's modulus (E) and elastic anisotropy (A), from which other properties such as hardness and ductility can be determined. In this study, the calculated elastic constants will be used to initially outline the general mechanical stability of each A15 X_3Ru structures based on the Born mechanical stability criteria [19]. In addition, the elastic constants can be used to measure the tensile, shear strength of materials, and provide important information on the bonding characteristics between the adjacent crystal atoms and the long-ranged elastic interaction between various dislocations [20].

2.6.1 Bulk modulus

Bulk Modulus (B) is a measure of the material's resistance to uniform compression. A high value of bulk modulus B indicates that a material resists compression, while a low bulk modulus imply that a material may be easily compressed. For cubic crystal structures, B is defined as

$$B = B_H = \left(\frac{B_V + B_R}{2}\right) \tag{14}$$

where

$$B = B_R = B_V = \left(\frac{C_{11} + 2C_{12}}{3}\right) \tag{15}$$

with B_R, B_V and $B = B_H$ being the Bulk modulus for Reuss, Voigt and Hill approximations [21].

2.6.2 Shear modulus

The shear modulus (G) of a material describes its response to shear stress, and is a measure of a material's stiffness. For cubic structures, G can be expressed as:

$$G = G_H = \left(\frac{G_V + G_R}{2}\right) \tag{16}$$

where the G_R and G_V are the Reuss and Voigt bounds [22], with

$$G_V = \left(\frac{C_{11} - C_{12} + 3C_{44}}{5}\right) \tag{17}$$

and

$$G_R = \left(\frac{(5(C_{11} - C_{12})C_{44})}{(4C_{44} + 3(C_{11} - C_{12}))}\right) \tag{18}$$

2.6.3 Young's modulus

Young's modulus (E) describes the material's strain response to uniaxial stress in the direction of this stress, and it can be written as:

$$E = \left(\frac{9B_H G_H}{3B_H + G_H}\right) \tag{19}$$

2.6.4 Elastic anisotropy

Anisotropic behavior is very important in engineering science as well as crystal physics due to its high relation with micro-cracks in materials. In calculating elastic anisotropy, more information about a material will result such as micro-cracks, phase transformation, precipitation and dislocation dynamics [23]. The elastic anisotropy (A) assist to distinguish the micro-cracks in different materials [24–26] and can be understood by calculating the anisotropic factor (A) for cubic structures as follows:

$$A = \left(\frac{2C_{44} + C_{12}}{C_{11}}\right) \tag{20}$$

2.6.5 Ductility

Ductility is the ability of a material to undergo plastic deformation before rapture. It is an important property for material engineering design. An empirical relation linking materials ductility and its elastic moduli (B/G) was proposed by Pugh [27], in which the critical value separating ductile and brittle materials is around 1.75; if B/G > 1.75, the material is ductile, otherwise it is brittle. Another classification rule was given by Frantsevich et al. [28] to distinguish brittleness and ductility by Poisson's ratio:

$$v = \left(\frac{3B_H - 2G_H}{(2(3B_H + G_H))} \right) \tag{21}$$

The critical value for Poisson's ratio is 1/3. For brittle materials, the Poisson's ratio is less than 1/3.

2.7 Density

Density is a vital tool used to characterize light/heavy weight materials. The weight of a material plays an essential role especially in rotating components. Therefore, it will be of interest to evaluate the density of the proposed X_3Ru alloys for lightweight (high temperature) structural applications. Density will be calculated from the Eq. (22) below:

$$\rho^{cal} = \left[\frac{M_W * N}{Vol * A_0} \right] \tag{22}$$

where *Vol* is the volume of the unit cell, M_W is the average molecular weight of the elements in the unit cell, N is the total number of atoms and A_0 is the Avogadro's number (6.022 $X10^{23}$).

2.8 Melting point temperature

The melting point is the temperature at which a material changes from the solid to the liquid state. In other words, the vapor pressure of the solid and the liquid are equal at its melting point temperature. The melting temperature (*Tm*) of a material depends on its mechanical properties, and it follows a linear relationship with its elastic constants [29–32]. For cubic systems, the melting point temperature is given by:

$$T_m = 553K + \left(\frac{591K}{Mbar} \right) * C_{11}(Mbar) \pm 300K \tag{23}$$

2.9 Computational details

The Cambridge Serial Total Energy Package (CASTEP) code [33] based on DFT was employed to examine the behavior of cubic A15 X_3Ru (X = Sc, Ti, V, Cr, Mn, Fe, Co, Cu, Ni and Zn) compounds. The calculations were carried out with plane wave pseudo-potentials [34] built within the generalized gradient approximation (GGA) to represent the valence core interactions. In the present calculations, the GGA + Hubbard U [35, 36] model for A15 compounds are used for electron–electron interaction. The wave functions are expanded in the plane waves up to a kinetic energy cutoff of 800 eV, while well converged 15×15×15 k-point sampling by Monkhorst-Pack [37] was used for integration over the Brillouin zone for all the A15 structures. This plane-wave energy cut-off value is convenient for electronic band structures and density of states. The equilibrium lattice parameters have been computed by minimizing the geometry of the crystal using the well-converged k-points allowing the total energy and forces to converge to less than 1 meV/atom and 0.03 eV/Å. For the elastic constants, the stress–strain method was applied on all A15 with cubic symmetry of C_{11}, C_{12} and C_{44} elastic constants. The Voigt, Reuss and Hill average has been applied for bulk (B), shear (G) and Young (E)'s modulus [38].

3. Results and discussion

3.1 Structural parameters and heats of formation

Ruthenium based transition metal alloys belong to the family of A15 X_3Z structures which consist of X atoms that occupy six equivalent positions in c-site (0.25, 0, 0.5) and Z atoms that occupy bcc positions (0, 0, 0), as illustrated by **Figure 1** in section 2.1.

Table 1 indicates the calculated lattice constants, heats of formation and magnetic moments of A15 X_3Ru alloys (X = Sc, Ti, V, Cr, Mn, Fe, Co, Cu, Ni, Zn). It can be seen in X_3Ru alloys that consist of transition metal atoms in the middle of the 3d series have lower lattice constants compared to those early or late in the series, in consistent with the trends of atomic radii of transition metal atoms across the 3d series. The computed lattice constants for Cr_3Ru (5.59 Å) and Ni_3Ru (4.84 Å) structures are comparable with those obtained from other theoretical investigations Cr_3Ru (4.61 Å, 4.623 Å and 4.62 Å) [14, 39, 40] and Ni_3Ru (4.57 Å) [39], confirming the accuracy of our results. The slight deviations between our calculated lattice constants and previous theoretical data can be attributed to the use of different plane wave cutoff energies and k-points grid. In this paper we have applied deeper energy cutoff (800 eV) and k-points grid of 15 x 15 x 15 compared to previous calculations. The heat of formation ΔH_f was calculated using Eq. (24) for all the structures as:

$$\Delta H_f = \left[\frac{E(X_3Ru) - aE_{Ru}^g - bE_X^g}{a + b} \right] \qquad (24)$$

Where $E(X_3Ru)$ is the total energy of the system, E_{Ru}^g and E_X^g are the energies of each individual metal species in their ground states, a and b are the number of atoms for individual metals and X = Sc, Ti, V, Cr, Mn, Fe, Co, Cu, Ni and Zn. A negative value ΔH_f indicates stability while the positive value of ΔH_f shows instability. It was found that Mn_3Ru have negative heats of formation, indicating that the alloy is thermodynamic stable. This result indicates a possibility of synthesizing Mn_3Ru experimentally due to the existence of the A15 Cr_3Ru phase [41]. Other

| System	Lattice constant (Å)	Heat of formation (eV/atom)	Magnetic Moment (μ_B/atom)	Density $\rho = g/cm^3$	X-Ru bond length (Å)
Sc_3Ru	5.51	1.09	0.01	4.48	3.081
Ti_3Ru	5.15	0.88	0.27	5.94	2.88
V_3Ru	5.15	0.79	0.03	6.16	2.881
Cr_3Ru	5.59	0.89	0.22	4.88	3.126
Mn_3Ru	5.37	−-0.64	2.59	5.72	2.999
Fe_3Ru	4.9	1.34	1.58	7.57	2.741
Co_3Ru	4.9	1.41	1.7	7.85	2.738
Ni_3Ru	4.84	2.11	1	8.13	2.704
Cu_3Ru	4.97	1.12	0.4	7.89	2.779
Zn_3Ru	5.24	1.02	0.01	6.86	2.929

Table 1.
Calculated lattice constants of X_3Ru (X = Cr, Sc, Ti, V, Mn, Fe, Cu, Ni, Co and Zn) unit cell as well as the heats of formation, magnetic moment, density and the X-Ru bond-length of A15 structures.

structures such as Sc_3Ru, Ti_3Ru, V_3Ru, Cr_3Ru, Fe_3Ru, Co_3Ru, Ni_3Ru, Cu_3Ru and Zn_3Ru have positive heats of formation indicating that they are thermodynamically unstable, hence synthesis may be difficult. However, it has been suggested previously [14, 42, 43] that doping lowers the heats of formation in some materials, which may make it possible to synthesize some of these structures. Importantly, we find a strong direct correlation between the heats of formation of the X_3Ru alloys and their magnetic moments, with higher magnetic moments corresponding to more stable alloys, as illustrated in **Figure 4**. This can be attributed to strong metallic bonding in transition metals arising from the delocalized electrons.

Similarly the larger atomic radii difference between the Ru atom and transition metal atoms results in crystal strain which has a positive impact on the overall magnetic moment, as summarized in **Table 2**. The density of an alloy plays an important role in determining its use in lightweight applications, such as the aerospace industry. We have therefore, evaluated the density of the proposed X_3Ru alloys for lightweight (high temperature) structural applications. From **Table 1**, we note that X_3Ru alloys with small lattice constants have higher densities and the results are consistent with Eq. (22). However, the density of the most stable alloy Mn_3Ru ($5.72\,g/cm^3$), is slightly lower than that of $L1_2$ Ni_3Al ($6.14\,g/cm^3$) [44], which is commonly used in the aerospace industry. Therefore, the application of these alloys with high densities may be limited. Whereas, Mn_3Ru may be a possible candidate for aerospace application due to lower density.

3.2 Electronic and magnetic properties

The calculated magnetic moments and the stability of intermetallic alloys can be rationalized from their electronic properties [45]. **Figure 5** presents the projected spin-polarized density of states (PDOS) of X_3Ru (X = Sc, Ti, V, Cr, Mn, Fe, Co, Ni, Cu and Zn) alloys. It can be seen that the spin up and spin down bands are symmetric in Sc, Ti, V, Cr, Cu and Zn systems, with no net spin polarization. This symmetric balance of the spin up and spin down bands leads to a cancelation of the magnetic moment associated with electronic spin, thus explaining the zero (or negligible) calculated magnetic moments (**Table 1**). On the other hand, the density of states in Mn, Fe, Co and Ni are spin-polarized, which explains the origin of the non-zero calculated magnetic moments in these systems. The predicted magnetic
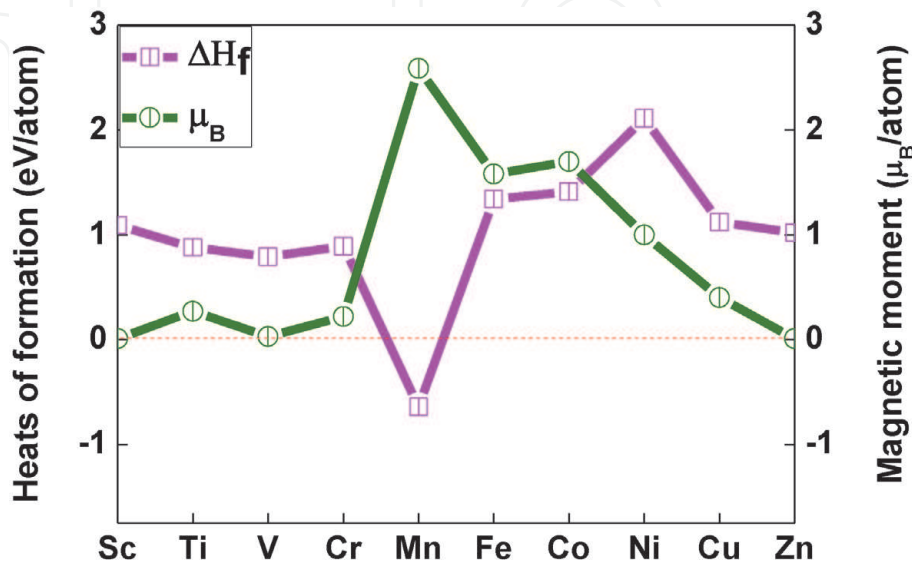
Figure 4.
A comparison of the calculated heats of formation (eV/atom) and magnetic moment (μ_B/atom) of X_3Ru (X = Sc, Ti, V, Cr, Mn, Fe, Ni, Co, Cu and Zn) alloys.

Element	Atomic radii (pm)	Relative Ru-X atomic radii (pm)	Magnetic moments/ atom	Relative Ru-X magnetic moment (Ru = 0.00μ$_B$/ atom)	Electronic configuration	No: of unpaired spin
Sc	162	16	0.95	0.95	[Ar] 3d^{1}4s^2	2
Ti	147	31	2.09	2.09	[Ar] 3d^{2}4s^2	1
V	134	44	0.79	0.79	[Ar] 3d^{3}4s^2	0
Cr	128	50	4.93	4.93	[Ar] 3d^{5}4s^1	2
Mn	161	17	5	5	[Ar] 3d^{5}4s^2	2
Fe	156	22	2.64	2.64	[Ar] 3d^{6}4s^2	3
Co	152	26	1.68	1.68	[Ar] 3d^{7}4s^2	4
Ni	159	29	1.28	1.28	[Ar] 3d^{8}4s^2	5
Cu	145	33	0	0	[Ar] 3d^{10}4s^1	3
Zn	142	36	0	0	[Ar] 3d^{10}4s^2	3

Table 2.
The atomic radii, atomic radii difference, magnetic moments, electronic configuration and number of paired electrons of 3d transition metal from Sc-Zn bonded with central Ru atom.

moments in these compounds could lead to novel applications such as spintronics and spin injections.

The total density of states (DOS) can be used to investigate the atomic bonding character of Ru-based alloys [45]. It is clear that the bonding character mainly arises from the hybridization of X-*d* and Ru-*d* below the Fermi energy (−4 to -1 eV). Around the Fermi energy, from the spin up and down channels, the most visible feature is the presence of a valley known as the pseudo-gap, which indicates cova-lent bonding [46, 47] in these compounds. The pseudo-gap exist due to strong hybridization in X-*d* and Ru-*d* states and separates the bonding states from the anti-bonding states. The phase stability of intermetallic compounds is dependent on the location and magnitude of the DOS at the Fermi energy N(E$_f$) [48–50], with lower N(E$_f$) corresponding to a more stable phase [51]. The electronic properties can be related with the heats of formation, Mn$_3$Ru structure have less density of states at the Fermi and therefore, it is most stable. This result explains the calculated heats of formation results of Mn$_3$Ru discussed in section 3.1 above, where Mn$_3$Ru is ther-modynamically stable and this attributes to its lowest heats of formation.

3.3 Elastic properties

Elastic constants are parameters that express the mechanical behavior of the materials within the stress range that the materials exhibit elastic behavior. In science and technology, they are essential physical quantities to determine the mechanical properties. The elastic constants C$_{ijs}$ of A15 X$_3$Ru (X = Sc, Ti, V, Cr, Mn, Fe, Co, Ni, Cu and Zn) compounds are shown in **Table 3**. For the cubic X$_3$Ru compounds, the condition of Born mechanical stability [52] follows the equations:

$$C_{44} > 0, C_{12} > 0, C_{11} - C_{12} > 0 \qquad (25)$$

The elastic constants of Cr$_3$Ru satisfies the above formulae, whilst other struc-tures do not and this attributes to $C_{44} < 0$ and $C_{12} > 0$. For these elastic constants, the bigger the elastic constant C_{11} is, the stronger the linear compression resistance
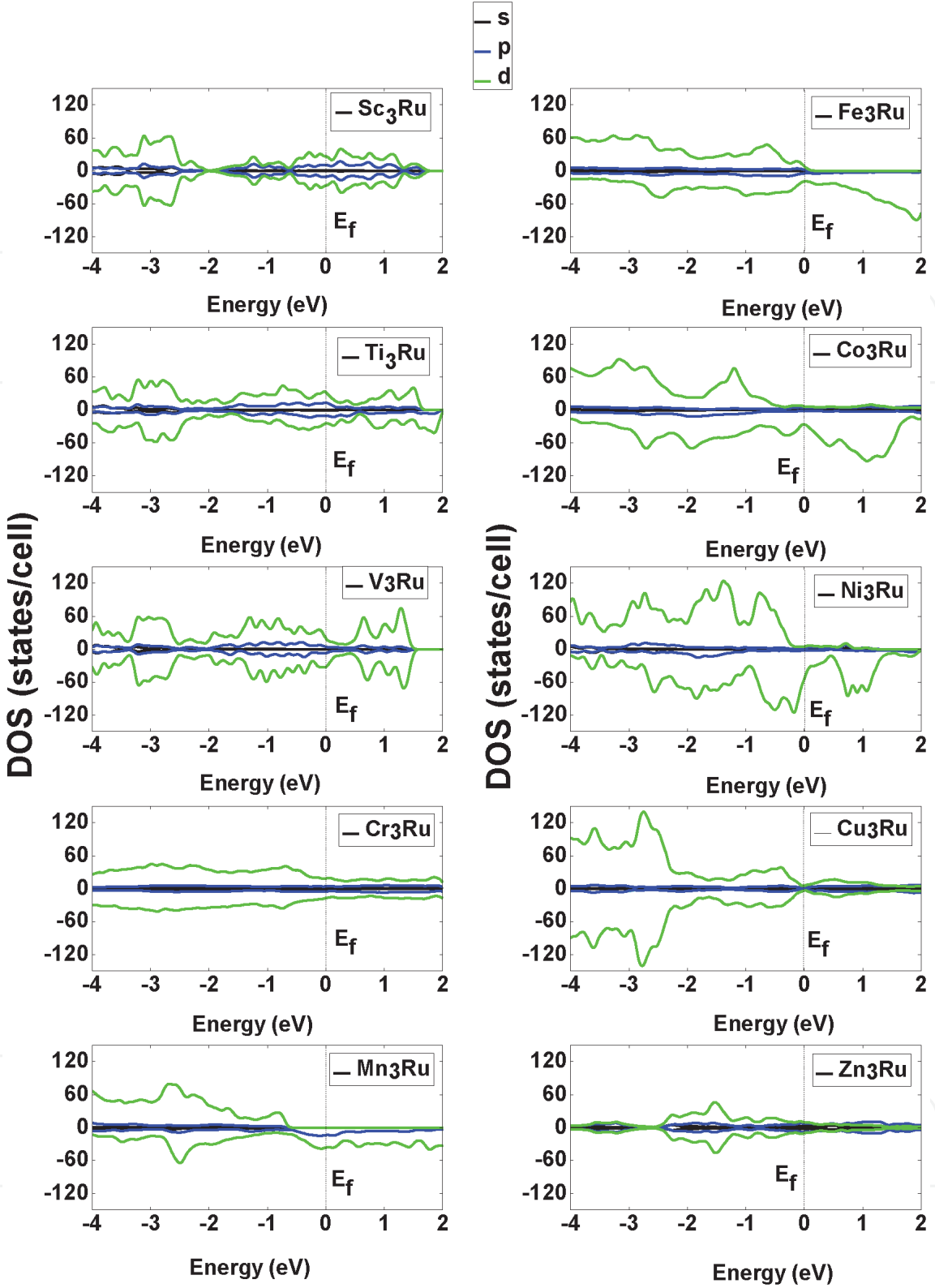
Figure 5.
Partial density of states of binary X_3Ru (X = Sc, Ti, V, Cr, Mn, Fe, Co, Ni, Cu and Zn). The Fermi energy is taken as zero energy, indicated with the vertical dotted line.

along the X-axis direction [53]. Ti_3Ru has the strongest resistance to the compressibility among all the structures, due to the largest C_{11} (1061 GPa) value [54]. The elastic constant C_{44} reflects the degree of shear resistance in the (100) plane and affects the hardness of solid materials indirectly [55]. Fe_3Ru has a larger C_{44} (137 GPa) suggesting a stronger ability to resist shear distortion in (100) plane. The elastic modulus such as (bulk modulus *B*, shear modulus *G* and Young's modulus *E*), Poisson's ratio υ, melting temperature Tm and anisotropic factor are used to

determine the mechanical properties. The elastic moduli of A15 X_3Ru (X = Sc, Ti, V, Cr, Mn, Fe, Co, Ni, Cu and Zn) structures are shown in **Table 3**. Bulk modulus reflects the incompressibility of solid materials. The stronger incompressibility in solid material correspond to larger bulk modulus. Under constant volume conditions, the shear modulus denotes the deformation resistance of solid materials, whilst the Young's modulus offers a measure of the stiffness of a solid.

The Fe_3Ru structure indicates larger bulk (1060 GPa), shear (209 GPa) and Young's modulus (672 GPa) as shown in **Table 3** and therefore shows stronger resistance to compressibility, shear deformation and stiffness. It is noted that the X_3Ru (X = Sc, V, Co, Ni, Cu and Zn) structure have negative shear modulus and Young's modulus. Furthermore, Co indicates the smallest negative shear modulus (-991.0 GPa) and Young's modulus ($-2.2*10^5$ GPa) indicating instability associated with phase change. This instability is also observed in ferro-elastic phase transformation [56]. The negative elastic modulus is due to Landau theory [57] when two local minima form in a strain energy function. Besides, solids with negative elastic modulus can be stabilized with sufficient constraint. The ratio of B/G is larger than 1.75 and predicts ductile behavior in a solid material [27]. Otherwise, it will exhibit the brittle behavior. Similar trend is expected in Poisson's ratio [28], which refers to ductile compounds normally with a large ($\upsilon > 0.3$) and lastly, positive Cauchy pressure (C_{11}-C_{12}) [58, 59] shows that the given material is expected to be ductile whilst negative Cauchy pressure indicates brittleness as shown in **Table 3**.

The X_3Ru (X = Ti, Mn, Cr and Fe) structures are ductile due to B/G values greater than 1.75 whilst, Sc_3Ru, Co_3Ru, Ni_3Ru, Cu_3Ru and Zn_3Ru are brittle. It is noted that Cr_3Ru (19.6) is more ductile indicated in **Table 3** and possess high fracture toughness. This is in agreement with the Poisson's ratio and Cauchy pressure results discussed. A positive Cauchy pressure in Mn_3Ru (52 GPa) and Cr_3Ru (241 GPa) is observed with B/G ratio of 16 and 19.6 and Poisson's ratio of (0.5 and 0.5) indicating ductile characteristics. Similar trend of results are shown in A15 XNb_3 (X = Al, Ge, Si, Sn, Pt and Ir) studies, and ductility can be attributed by positive Cauchy pressure [60, 61].

System	C_{11}	C_{12}	C_{44}	B	G	E	B/G	C_{12}-C_{44}	υ	T_m (K)	A
	GPa	GPa	GPa	GPa	GPa	GPa		GPa	GPa		
Sc_3Ru	78	104	33	95	−33	−113	−2.9	71	0.7	1014	2.2
Ti_3Ru	1061	74	−34	403	58	167	7	108	0.4	6824	0.01
V_3Ru	242	95	−621	144	−60	−209	−2.4	716	0.7	1983	−4.70
Cr_3Ru	336	245	4	275	14	40	19.6	241	0.5	2539	0.8
Mn_3Ru	145	48	−4	80	5	14	16	52	0.5	1410	0.3
Fe_3Ru	−1328	−922	137	1060	209	672	5.1	−1059	0.6	−7295	0.5
Co_3Ru	765	120	−340	335	−991	−2.2x10⁵	−0.3	460	110	5074	−0.70
Ni_3Ru	91	102	−163	98	−57	−210	−1.7	265	0.9	1091	−2.50
Cu_3Ru	156	54	−43	88	−85	−374	−1.0	97	1.2	1475	−0.20
Zn_3Ru	79	40	−19	53	−47	−198	−1.1	59	1.1	1020	0.03

Table 3.
Calculated elastic constants (C_{ij}), Moduli (average B, G, E_{VRH}), Poisson's ratio (υ), Shear moduli (C), the ratio of Bulk to Shear (B/G), Cauchy pressure (C_{12}-C_{44}), Melting temperature (T_m) and elastic anisotropy (A). All elastic constants and Moduli are in GPa.

3.4 Melting temperatures (T_m) of A15 Ru-based alloys

To assess the potential of high-temperature application of X_3Ru structures, we have calculated their melting temperatures based on the elastic constants C_{ij}, [30, 32] as presented in **Table 3**. It is evident that Ti_3Ru (6824 K) structure possesses high melting point whereas Fe_3Ru (−7295 K) has a low melting point. This attributes to the elastic constant C11 factor in these structures that leads to variation in melting temperatures. The calculated melting temperatures (T_m) of several studied X_3Ru are in the same range as Nb_3Al (2333 K) [1] and Ni_3Al (1668 K) [44] which are obtained experimentally and theoretically. The calculated T_m of V_3Ru (1983 K), Cr_3Ru (2539 K), Co_3Ru (5074 K) and Ti_3Ru (6824) are greater than the T_m of Ni_3Al (1668 K).

3.5 Elastic anisotropy

If the anisotropic index A is close to 1 (unity) respectively, the solid materials are predicted to be isotropic. Otherwise, it will be anisotropic. The anisotropic factors (A) of X_3Ru (X = Sc, Ti, V, Cr, Mn, Fe, Co, Ni, Cu and Zn) ranges from −4.7 to 2.2 respectively. It is clear that all the X_3Ru (X = Sc, Ti, V, Cr, Mn, Fe, Co, Ni, Cu and Zn) values have deviated away from unity; thus, the structures are anisotropic.

4. Conclusion

Using first principles density functional theory calculations, we have investigated the structural, electronic, magnetic and elastic properties of X_3Ru (X = Sc, Ti, V, Cr, Fe, Co, Cu and Zn) binary alloys in search of potential materials for high temperature structural application. The negative heat of formation in Mn_3Ru has been observed, indicating that the system is thermodynamically stable compared to other studied X_3Ru alloys that exhibited positive heats of formation. The total partial density of states show a strong overlap between the valence and conduction bands in Sc_3Ru, Ti_3Ru, V_3Ru, Cr_3Ru Fe_3Ru, Cu_3Ru and Zn_3Ru indicating that these systems are metallic, whilst X_3Ru (X = Mn, Co and Ni) are found to be half-metallic. Furthermore, Cr_3Ru is known to exist experimentally, on the other hand, no experimental data has been reported on all the remaining X_3Ru systems. The elastic constants and related mechanical parameters such as bulk modulus, shear modulus, Young's modulus, B/G ratio and Poisson's ratio, melting temperatures and anisotropy factor are calculated. According to the elastic stability criteria, all X_3Ru structures are mechanically unstable except Cr_3Ru with highest B/G ratio of 19.6. The calculated anisotropic factor indicates that all the X_3Ru (X = Sc, Ti, V, Cr, Mn, Fe, Co, Ni, Cu and Zn) are anisotropic. Co_3Ru, Fe_3Ru, Ni_3Ru and Mn_3Ru possess magnetic moments of 1.70, 1.58, 0.97 and 2.59 u_B, respectively, while Sc_3Ru, Ti_3Ru, V_3Ru, Cu_3Ru, Cr_3Ru and Zn_3Ru are non-magnetic. The results for stable Mn_3Ru with high magnetic moment could pave way for experimental realization (synthesis) of this material. Finally, the thermodynamic stable alloy Mn_3Ru is predicted to be a good candidate for high temperature and spintronic applications.

Author details

Bhila Oliver Mnisi*, Evans Moseti Benecha and Meriam Malebo Tibane
Department of Physics, University of South Africa, Johannesburg, South Africa

*Address all correspondence to: bhila.oliver00@gmail.com

IntechOpen

References

[1] C.T. Sims, N.S. Stoloff, W.C. Hagel, superalloys II, Wiley New York, 1987.

[2] Y. Yamabe-Mitarai, Y. Gu, C. Huang, R. Völkl, H. Harada, Platinum-group-metal-based intermetallics as high-temperature structural materials, JOM. 56 (2004) 34–39.

[3] P. Caron, High y'solvus new generation nickel-based superalloys for single crystal turbine blade applications, Superalloys. 2000 (2000) 737–746.

[4] P.K. Liao, K.E. Spear, T.B. Massalski, Binary alloy phase diagrams, ASM Int. Mater. Park. Ohio. 1 (1990) 557–559.

[5] R. Süss, L.A. Cornish, U. Glatzel, Comparison of experimentally determined and CALPHAD-determined results of the Pt-Cr-Ru System, CALPHAD XXXIII Progr. Abstr. 34 (2004).

[6] W. Wopersnow, C.J. Raub, The Alloys of Ruthenium with Palladium and Chromium as well as with Some Other Transition Metals, Metall. 33 (1979) 1261–1265.

[7] B.M. Venkatraman, J.P. Neumann, The Cr-Ru (Chromium-Ruthenium) System 51.996 101.07, Bull. Alloy Phase Diagrams. 8 (1987) 109–112.

[8] M. Jahnátek, O. Levy, G.L.W. Hart, L.J. Nelson, R. V Chepulskii, J. Xue, S. Curtarolo, Ordered phases in ruthenium binary alloys from high-throughput first-principles calculations, Phys. Rev. B. 84 (2011) 214110.

[9] A.R. Miedema, A.K. Niessen, F.R. De Boer, R. Boom, W.C.M. Matten, Cohesion in metals: transition metal alloys, Report, Philips Res. Lab. Eindhoven, Netherlands. FR Boer, R. Boom, WCM Mattens, AR Miedema, AK Niessen Cohes. Met. Transit. Met. Alloy. North-Holl. Publ. Co., Amsterdam. (1989).

[10] D.R. Lide, CRC handbook of chemistry and physics, CRC Boca Raton, 2012.

[11] R.A. Hobbs, L. Zhang, C.M.F. Rae, S. Tin, Mechanisms of topologically close-packed phase suppression in an experimental ruthenium-bearing single-crystal nickel-base superalloy at 1100 C, Metall. Mater. Trans. A. 39 (2008) 1014–1025.

[12] A. Sato, H. Harada, T. Yokokawa, T. Murakumo, Y. Koizumi, T. Kobayashi, H. Imai, The effects of ruthenium on the phase stability of fourth generation Ni-base single crystal superalloys, Scr. Mater. 54 (2006) 1679–1684.

[13] A.C. Yeh, S. Tin, Effects of Ru and Re additions on the high temperature flow stresses of Ni-base single crystal superalloys, Scr. Mater. 52 (2005) 519–524.

[14] M.M. Tibane, Phase stability study of Pt-Cr and Ru-Cr binary alloys, (2011).

[15] M. Born, R. Oppenheimer, Zur quantentheorie der molekeln, Ann. Phys. 389 (1927) 457–484.

[16] P. Hohenberg, W. Kohn, Inhomogeneous electron gas, Phys. Rev. 136 (1964) B864.

[17] S. Tosoni, C. Tuma, J. Sauer, B. Civalleri, P. Ugliengo, A comparison between plane wave and Gaussian-type orbital basis sets for hydrogen bonded systems: Formic acid as a test case, J. Chem. Phys. 127 (2007) 154102.

[18] X. Li, H. Zhang, S. Lu, W. Li, J. Zhao, B. Johansson, L. Vitos, Elastic properties of vanadium-based alloys from first-principles theory, Phys. Rev. B. 86 (2012) 14105.

[19] M. Born, On the stability of crystal lattices. I, in: Math. Proc. Cambridge

Philos. Soc., Cambridge University Press, 1940: pp. 160–172.

[20] C.L. Fu, M.H. Yoo, Electronic structure and mechanical behavior of transition-metal aluminides: A first-principles total-energy investigation, Mater. Chem. Phys. 32 (1992) 25–36.

[21] R. Hill, The elastic behaviour of a crystalline aggregate, Proc. Phys. Soc. Sect. A. 65 (1952) 349.

[22] A. Reuss, Calculation of the flow limits of mixed crystals on the basis of the plasticity of monocrystals, Z. Angew. Math. Mech. 9 (1929) 49–58.

[23] X. Liu, Q. Feng, B. Tang, J. Zheng, Z. Zheng, W. Zhou, J. Tian, J. Wang, First-principles calculations of mechanical and thermodynamic properties of tetragonal Be 12 Ti, RSC Adv. 9 (2019) 5302–5312.

[24] Z.Q. Lv, Z.F. Zhang, Q. Zhang, Z.H. Wang, S.H. Sun, W.T. Fu, Structural, electronic and elastic properties of the Laves phases WFe2, MoFe2, WCr2 and MoCr2 from first-principles, Solid State Sci. 56 (2016) 16–22.

[25] V. Tvergaard, J.W. Hutchinson, Microcracking in ceramics induced by thermal expansion or elastic anisotropy, J. Am. Ceram. Soc. 71 (1988) 157–166.

[26] H. Fu, D. Li, F. Peng, T. Gao, X. Cheng, Ab initio calculations of elastic constants and thermodynamic properties of NiAl under high pressures, Comput. Mater. Sci. 44 (2008) 774–778.

[27] S.F. Pugh, XCII. Relations between the elastic moduli and the plastic properties of polycrystalline pure metals, London, Edinburgh, Dublin Philos. Mag. J. Sci. 45 (1954) 823–843.

[28] I.N. Frantsevich, F.F. Voronov, S.A. Bokuta, Elastic Constants and Elastic Moduli of Metals and Insulators Handbook, edited by IN Frantsevich

(Naukova Dumka, Kiev, 1983), Google Sch. (1983) 60–180.

[29] A.I. Popoola, Computational study of noble metal alloys, (2014).

[30] D.J. Skinner, M. Zedalis, Elastic modulus versus melting temperature in aluminum based intermetallics, Scr. Metall. 22 (1988) 1783–1785.

[31] M. Blackman, On the calculation of characteristic temperatures from the Elastic constants, London, Edinburgh, Dublin Philos. Mag. J. Sci. 42 (1951) 1441–1442.

[32] M.E. Fine, L.D. Brown, H.L. Marcus, Elastic constants versus melting temperature in metals, Scr. Metall. 18 (1984) 951–956.

[33] S.J. Clark, M.D. Segall, C.J. Pickard, P.J. Hasnip, M.I.J. Probert, K. Refson, Mike C Payne, First principles methods using CASTEP, Zeitschrift Fur Krist. 220 (2005) 567–570. https://doi.org/10.1524/zkri.220.5.567.65075.

[34] D. Vanderbilt, Soft self-consistent pseudopotentials in a generalized eigenvalue formalism, Phys. Rev. B. 41 (1990) 7892.

[35] J. Perdew, K. Burke, M. Ernzerhof, PBE and PBE0, Phys. Rev. Lett. 77 (1996) 3865–3868. https://doi.org/10.1103/PhysRevLett.77.3865.

[36] A.I. Liechtenstein, V.I. Anisimov, J. Zaanen, Density-functional theory and strong interactions: Orbital ordering in Mott-Hubbard insulators, Phys. Rev. B. 52 (1995) R5467.

[37] H.J. Monkhorst, J.D. Pack, Special points for Brillouin-zone integrations, Phys. Rev. B. 13 (1976) 5188.

[38] V. Petrman, J. Houska, Trends in formation energies and elastic moduli of ternary and quaternary transition metal

nitrides, J. Mater. Sci. 48 (2013) 7642–7651.

[39] N.I. Medvedeva, A.L. Ivanovskii, Ab-initio study of Re and Ru effect on stability of TCP nanoparticles in Ni-based superalloys, Наносистемы: Физика, Химия, Математика. 5 (2014).

[40] B.O. Mnisi, E.M. Benecha, H.R. Chauke, P.E. Ngoepe, M.M. Tibane, Effect of transition metal doping on Cr–Ru alloys using first principles approach, Bull. Mater. Sci. 43 (2020) 1–9.

[41] Y.F. Gu, H. Harada, Y. Ro, T. Kobayashi, Microstructural Evolution and Mechanical Properties of Cr-Ru Alloys, 36 (2005) 577–582.

[42] A. Continenza, G. Profeta, S. Picozzi, Transition metal doping and clustering in ge, Appl. Phys. Lett. 89 (2006) 202510.

[43] F. Kong, R.C. Longo, M.-S. Park, J. Yoon, D.-H. Yeon, J.-H. Park, W.-H. Wang, K.C. Santosh, S.-G. Doo, K. Cho, Ab initio study of doping effects on LiMnO 2 and Li 2 MnO 3 cathode materials for Li-ion batteries, J. Mater. Chem. A. 3 (2015) 8489–8500.

[44] A.I. Popoola, J.E. Lowther, Computational Study of Platinum Group Superalloys, Int. J. Mod. Phys. B. 28 (2014) 1450066.

[45] J. Bai, J.M. Raulot, Y.D. Zhang, C. Esling, X. Zhao, L. Zuo, Crystallographic, magnetic, and electronic structures of ferromagnetic shape memory alloys Ni 2 XGa (X= Mn, Fe, Co) from first-principles calculations, J. Appl. Phys. 109 (2011) 14908.

[46] J. Xu, A.J. Freeman, Bandfilling and structural stability of trialuminides: YAl 3, ZrAl 3, and NbAl 3, J. Mater. Res. 6 (1991) 1188–1199.

[47] M. Krajci, J. Hafner, Covalent bonding and bandgap formation in

intermetallic compounds: a case study for Al3V, J. Phys. Condens. Matter. 14 (2002) 1865.

[48] B.H. Cheong, K.-J. Chang, First-principles study of the structural properties of Sn under pressure, Phys. Rev. B. 44 (1991) 4103.

[49] Y. Song, Z.X. Guo, R. Yang, D. Li, First principles study of site substitution of ternary elements in NiAl, Acta Mater. 49 (2001) 1647–1654.

[50] T. Hong, T.J. Watson-Yang, X.-Q. Guo, A.J. Freeman, T. Oguchi, J. Xu, Crystal structure, phase stability, and electronic structure of Ti-Al intermetallics: Ti 3 Al, Phys. Rev. B. 43 (1991) 1940.

[51] C. Yu, J. Liu, H. Lu, P. Li, J. Chen, First-principles investigation of the structural and electronic properties of Cu6− xNixSn5 (x= 0, 1, 2) intermetallic compounds, Intermetallics. 15 (2007) 1471–1478.

[52] D.C. Wallace, Thermodynamics of crystals, Courier Corporation, 1998.

[53] X. Gao, Y. Jiang, R. Zhou, J. Feng, Stability and elastic properties of Y–C binary compounds investigated by first principles calculations, J. Alloys Compd. 587 (2014) 819–826.

[54] X. Li, D. Chen, Y. Wu, M. Wang, N. Ma, H. Wang, Assessment on the structural, elastic and electronic properties of Nb3Ir and Nb3Pt: A first-principles study, AIP Adv. 7 (2017) 65012.

[55] G. Grimvall, Thermophysical properties of materials, Elsevier, 1999.

[56] E. Salje, Phase transitions in ferroelastic and co-elastic crystals, Ferroelectrics. 104 (1990) 111–120.

[57] F. Falk, Model free energy, mechanics, and thermodynamics of

shape memory alloys, Acta Metall. 28 (1980) 1773–1780.

[58] S. Ganeshan, S.L. Shang, H. Zhang, Y. Wang, M. Mantina, Z.K. Liu, Elastic constants of binary Mg compounds from first-principles calculations, Intermetallics. 17 (2009) 313–318.

[59] D.G. Pettifor, Theoretical predictions of structure and related properties of intermetallics, Mater. Sci. Technol. 8 (1992) 345–349.

[60] X. Li, D. Chen, Y. Wu, M. Wang, N. Ma, H. Wang, Assessment on the structural, elastic and electronic properties of Nb_3Ir and Nb_3Pt: A first-principles study, AIP Adv. 7 (2017) 065012. https://doi.org/10.1063/1.4986906.

[61] I. Papadimitriou, C. Utton, P. Tsakiropoulos, Ab initio investigation of the Nb–Al system, Comput. Mater. Sci. 107 (2015) 116–121.